iScience

CellPress
OPEN ACCESS

Article

Cavitation is the determining mechanism for the atomization of high-viscosity liquid

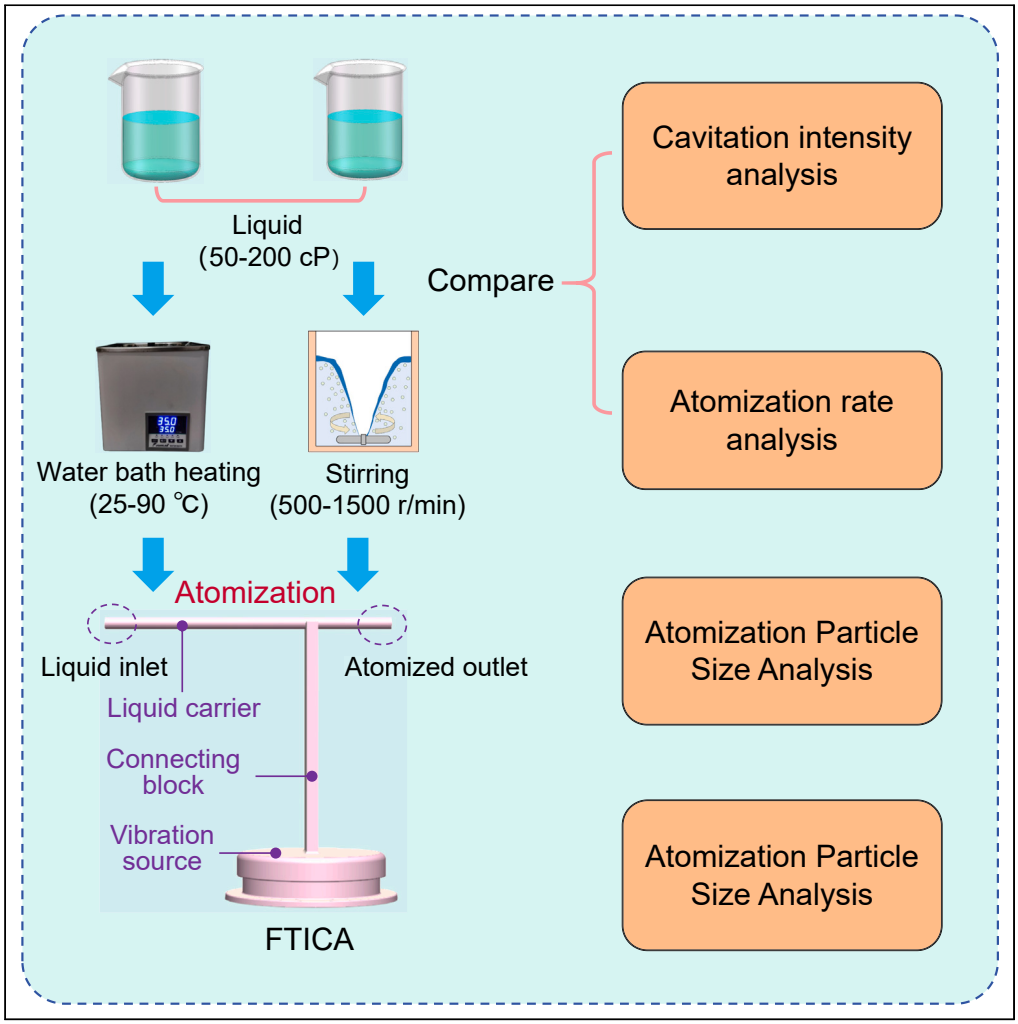

Zhenzhen Gui, Yaohua Zeng, Tang Xie, ..., Tao Zou, Fan Zhang, Jianhui Zhang

tzou@gzhu.edu.cn (T.Z.)
zhf_jd@gzhu.edu.cn (F.Z.)
zhangjh@nuaa.edu.cn (J.Z.)

Highlights

Cavitation is the determining factor for the atomization of high-viscosity liquids

Supporting the minority-endorsed cavitation hypothesis

FTICA is suitable for the atomization of biological proteins

The atomization of FTICA is a physical change

Gui et al., iScience 27, 110071
June 21, 2024
https://doi.org/10.1016/j.isci.2024.110071

iScience

CellPress
OPEN ACCESS

Article

Cavitation is the determining mechanism for the atomization of high-viscosity liquid

Zhenzhen Gui,[1] Yaohua Zeng,[1] Tang Xie,[1] Bochuan Chen,[1] Jialong Wang,[1] Yuxin Wen,[1] Tian Tan,[1] Tao Zou,[1,2,*] Fan Zhang,[1,*] and Jianhui Zhang[1,3,*]

SUMMARY

Piezoelectric atomization is becoming mainstream in the field of inhalation therapy due to its significant advantages. With the rapid development of high-viscosity gene therapy drugs, the demand for piezoelectric atomization devices is increasing. However, conventional piezoelectric atomizers with a single-dimensional energy supply are unable to provide the energy required to atomize high-viscosity liquids. To address this problem, our team has designed a flow tube internal cavitation atomizer (FTICA). This study focuses on dissecting the atomization mechanism of FTICA. In contrast to the widely supported capillary wave hypothesis, our study provides evidence in favor of the cavitation hypothesis, proving that cavitation is the key to atomizing high-viscosity liquids with FTICA. In order to prove that the cavitation is the key to atomizing in the structure of FTICA, the performance of atomization is experimented after changing the cavitation conditions by heating and stirring of the liquids.

INTRODUCTION

Atomization is the physical process of breaking the continuity of a liquid by applying energy, which causes the original continuous liquid to split into enclosed tiny liquid particles (droplets). This process changes single-phase flow into multiphase flow. The common atomization methods are pure pressure atomization,[1–3] combined pressure and thermal atomization,[4–6] and piezoelectric ultrasonic atomization.[7,8] In the medical field, pure pressure pneumatic atomization and piezoelectric ultrasonic atomization are the typical methods because heating can easily damage the properties of medications. However, given that pure pressure pneumatic atomization has difficulty controlling the droplet size distribution, it cannot be applied in situations with high requirements for particle size. Piezoelectric ultrasonic atomization has a high energy conversion rate and utilization, controllable and small particle size distribution of atomized particles, low outlet rate of droplets, a simple structure, and low cost[9–14] and has become mainstream in the medical field. Meanwhile, piezoelectric ultrasonic atomization has also been widely used in biomedicine,[15–17] advanced mechanical engineering,[18–21] advanced nanomaterials,[22–25] and environmental protection.[26–28]

The piezoelectric ultrasonic atomizer is the key device in the medical field for inhalation medication delivery treatment. Compared with traditional oral, intramuscular, and intravenous medication delivery methods, inhalation medication delivery can be directly applied to the affected area, and the dosage and side effects are greatly reduced. It is often used in the treatment of respiratory diseases such as chronic obstructive pulmonary disease,[29,30] asthma,[31,32] and pneumonia.[33,34] In recent years, it has also been reported to be used for the treatment of lung cancer.[35–37] Transnasal mucosal passage through the blood–brain barrier for treating epilepsy has also been reported.[38] In particular, the increasing maturity of genetic engineering and gene therapy will make inhalation medication delivery an important modality in addition to oral, intramuscular injection, and vascular traditional medication delivery. Accordingly, the piezoelectric ultrasonic atomizer will also be the most important device for inhalation medication delivery.

In recent years, the introduction of exogenous normal genes into target cells by gene transfer technology to treat diseases caused by genetic abnormalities has been called gene therapy technology, which can treat difficult diseases such as cancer, thalassemia, and autoimmune diseases. Gene therapy has become the development trend of modern medicine,[39–43] and inhaled gene therapy is the current research area in the field of inhaled medication delivery.[44–46] Under the single-dimensional energy supply, achieving a high energy supply that is necessary for the atomization of high-viscosity liquids is difficult. Therefore, the currently used piezoelectric ultrasonic atomizer cannot atomize the liquid with a viscosity higher than 10 cP, which results in that most medications used for inhaled therapy are primarily aqueous.[47–49] In addition, gene therapy medications are DNA and mRNA molecules wrapped with polymers, peptide chains, and lipids in the outer layer; therefore, the viscosity of the medication is higher than 10 cP. Currently, the viscosity for the atomization of high-viscosity liquids is usually reduced by heating,[50] but the high temperature tends to denature the medication and

[1]School of Mechanical and Electrical Engineering, Guangzhou University, Guangzhou Higher Education Mega Center, 230 Wai Huan Xi Road, Guangzhou 510006, China
[2]Guangdong-Hong Kong-Macao Key Laboratory of Multi-scale Information Fusion and Collaborative Optimization Control of Complex Manufacturing Process, Guangzhou 510006, China
[3]Lead contact
*Correspondence: tzou@gzhu.edu.cn (T.Z.), zhf_jd@gzhu.edu.cn (F.Z.), zhangjh@nuaa.edu.cn (J.Z.)
https://doi.org/10.1016/j.isci.2024.110071

is therefore unsuitable for biomedical applications.[51] our team has proposed a two-dimensional vibration-coupled structure to supply high energy input to the liquid.[52] This study discusses the existing ultrasonic atomization mechanism to explore the atomization mechanism of the abovementioned atomizer.

Ultrasonic cavitation is the process in which minuscule bubbles implode upon experiencing rapid pressure changes, resulting in a forceful impact.[53,54] In previous studies, researchers generally agreed on two hypotheses for the mechanism of ultrasonic atomization[55]: the capillary wave hypothesis and the cavitation hypothesis. The capillary wave hypothesis is based on Taylor instability,[56] which suggests that the capillary wave of liquid consists of wave peaks and valleys. When the liquid is excited by ultrasonic vibration, the capillary wave peaks on the surface of the liquid will overcome their surface tension and escape into the air to form droplets. However, the cavitation hypothesis is usually applied to systems of high-frequency vibration and high-energy density. When the liquid is excited by high-frequency vibrations, the liquid close to the free liquid surface generates a powerful impact due to the collapse and explosion of cavitation nuclei (tiny bubbles) to spray droplets into the air. Researchers have developed various arguments regarding the two atomization mechanisms. In summary, most studies consider capillary waves as an important basis for ultrasonic atomization, and cavitation is considered an auxiliary effect or concomitant phenomenon.[57–59]

However, the atomization mechanism of such atomizers can no longer be explained using the two mechanisms discussed above because of the increasing variety of ultrasonic atomizers, such as mesh ultrasonic atomizers. Therefore, Friend et al. classified ultrasonic atomizers into two types based on the relationship between the meniscus and the wavelength of the capillary wave.[60] When the length of the meniscus is larger than half of the surface capillary wave length, the size of the atomized droplet is determined by the wavelength of the surface capillary wave. Otherwise, the size of the atomized droplet is determined by the mesh size. Thereafter, Zhang et al. further explained the atomization mechanism of a dynamic mesh ultrasonic atomizer using the dynamic cone angle principle.[61–63] Consequently, ultrasonic atomizers can be divided into surface acoustic wave atomizers and mesh ultrasonic atomizers (static mesh and dynamic mesh).

Our research team has proposed the FTICA, which uses two-dimensional vibration synthesis to achieve the atomization of high-viscosity liquids, but the atomization mechanism is different from the existing atomizers. The present study suggests that vibration leads to cavitation, which results in liquid atomization, and cavitation is the determining mechanism in the atomization of high-viscosity liquids, rather than a concomitant phenomenon in the atomization process. This study explores causal relationships between cavitation and atomization by facilitating cavitation by heating or stirring the liquid to prove the abovementioned point. The two treatments impact cavitation while not affecting vibration. Specifically, we explore the effect of changes in the cavitation threshold and the collapse pressure of the cavitation nucleus on the atomization efficiency by increasing the temperature and the liquid stirring rate.

First, the relationship between the atomization rate and liquid temperature is studied by heating the liquid, where the bidirectional effects of the cavitation threshold and cavitation nucleus collapse pressure on atomization are proposed. The experimental results prove that the cavitation threshold decreases with the increase in temperature, which makes cavitation more likely to occur. However, increasing temperature will also lead to a decrease in vapor pressure, which results in lower collapse pressure, such a reduction makes cavitation less likely to occur. The cavitation intensity first increases with the rise in temperature and then decreases, which is consistent with the experimental results of the atomization rate. Therefore, cavitation is the determining factor of atomization for FTICA. Meanwhile, the optimal atomization temperature for the FTICA is 40°C. Thereafter, the air content in the liquid is increased by raising the stirring rate. Then, the relationship between the atomization rate and the air content of the liquid is studied. The experimental results prove that the effect of the cavitation threshold is greater than the influence of the collapse pressure of the cavitation nucleus at stirring rates lower than 1500 r/min. The cavitation intensity increases with the stirring rate. This finding is consistent with the experimental results of the atomization rate, which is additional evidence that cavitation is the determining factor of atomization for FTICA. Moreover, the atomization rate reaches its maximum at a stirring rate of 1500 r/min.

In this study, experiments prove that cavitation is the determining mechanism for the atomization of high-viscosity liquids, and the atomization temperature of 40°C is close to the body temperature of living organisms. Furthermore, the Raman spectroscopy experiments proved that the chemical properties of FTICA did not change before and after atomization at the optimal temperature (40°C) and optimal stirring rate (1500 r/min), which determined the safety of FTICA. Therefore, the two optimal parameters are suitable for inhalation therapy of medicine.

In summary, this study attempts to find other dimensions of energy beyond the vibrational dimension to promote cavitation, where more energy is supplied to the FTICA by increasing the liquid temperature and stirring rate. From the experimental results, two pieces of evidence are found to prove that the change in the atomization rate is consistent with the change in the cavitation intensity. Therefore, cavitation is proven to be the determining mechanism for the atomization of high-viscosity liquids in FTICA and proved the correctness of the cavitation hypothesis. In this study, two optimal atomization conditions, 40°C and 1500 r/min, were identified. These conditions provide a theoretical basis for the application of FTICA in inhalation gene therapy and other fields.

RESULTS

Results of impedance measurements

The relationship between impedance and frequency at different temperatures is shown in Figure 1A, where the frequency range is from 300 kHz to 800 kHz. The experimental results show that the impedance does not change under different temperature conditions, and the minimum impedance frequency is 742 kHz. The relationship between impedance and frequency at different stirring rates is shown in Figure 1B. The experimental results show that the impedance does not change at different stirring rates, and the minimum impedance frequency is 742 kHz. The impedance analysis experiments indicate that changes in the properties of the liquid do not affect the impedance of the FTICA.

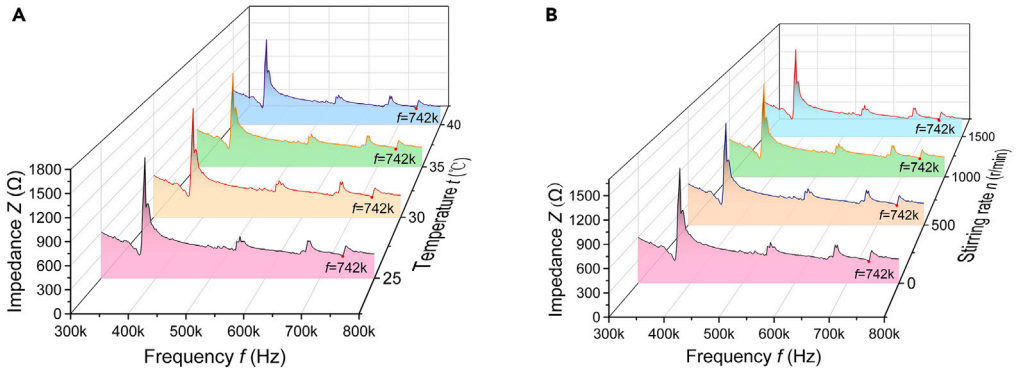

Figure 1. Results of impedance measurements of the FTICA

(A) results of impedance measurements of the FTICA after the passage of liquids with different temperatures.

(B) results of impedance measurements of the FTICA after the passage of liquid with different stirring rates.

Results of viscosity analysis

The relationship between liquid viscosity and temperature is shown in Figure 2A, the measured objects are four different viscosity liquids, the dynamic viscosity of 50 cP, 100 cP, 150 cP, 200 cP, the temperature range is 30°C–90°C, respectively. The experimental results show that the liquid viscosity decreases with the increase in temperature. When the liquid temperature is below 50°C, the viscosity decreases sharply, and after the liquid viscosity is above 50°C, the decreasing trend of viscosity becomes slower, the experimental results of liquid viscosity variation with temperature are consistent with Equation 19. The relationship between liquid viscosity and stirring rate is shown in Figure 2B, the measured objects are four different viscosity liquids, the dynamic viscosity of 50 cP, 100 cP, 150 cP, 200 cP, the stirring rate of the range of 250 r/min-1500 r/min. The experimental results show that there is no significant change in the fluid viscosity when the stirring rate is increased, which indicates that the viscosity of the liquid is not affected by the stirring rate.

Effect of temperature on atomization rate

The relationship between temperature and atomization rate at different dynamic viscosities is shown in Figure 3. The experimental results show that the atomization rate increases with temperature for the same viscosity and driving voltage. When the dynamic viscosity is 50 cP and the temperature is 40°C, the maximum atomization rate is 82.8 mg/min. As shown in Figure 3A, the temperature has the greatest effect on atomization. However, the effect of temperature change on the atomization rate decreases with the increase in viscosity. As shown in Figure 3D, when the dynamic viscosity of the liquid is 200 cP, the temperature has the minimum effect on the atomization rate, and the atomization rate is 0 for temperatures of 25°C and 30°C. Ultimately, the relationship between the AC signal drive voltage and the atomization rate is shown in Figure 3. The drive voltage affects the vibration amplitude of the FTICA, which in turn influences the cavitation intensity and achieves a higher atomization rate.

The abovementioned experimental results are consistent with Equations 1 and 21. Therefore, the viscosity and surface tension coefficient decrease with the increase in temperature. Such a decrease contributes to a lower cavitation threshold and makes cavitation more likely to occur.

However, continuous heating causes a tendency for the atomization rate to increase and then decrease, and the change in atomization rate during continuous heating is shown in Figure 4.

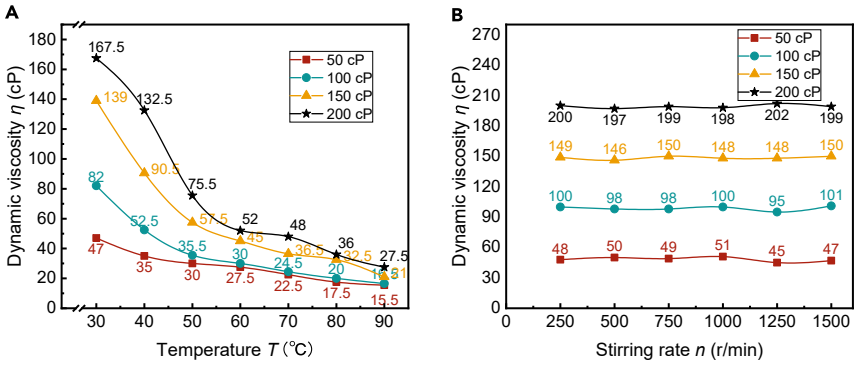

Figure 2. Results of viscosity analysis

(A) relationship between liquid viscosity and temperature.

(B) relationship between liquid viscosity and stirring rate.

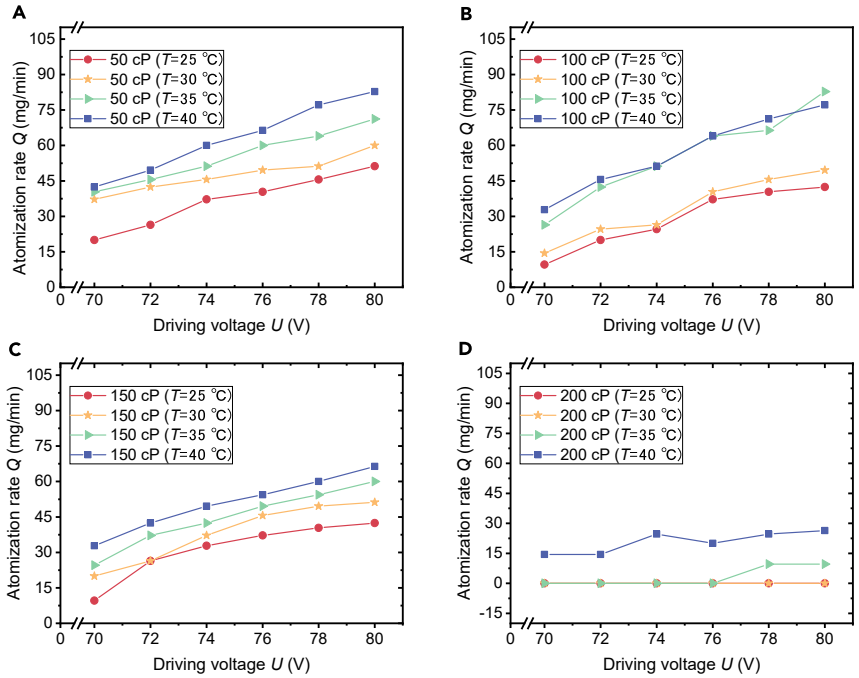

Figure 3. Relationship between temperature and atomization rate

(A) dynamic viscosity of 50 cP liquid.

(B) dynamic viscosity of 100 cP liquid.

(C) dynamic viscosity of 150 cP liquid.

(D) dynamic viscosity of 200 cP liquid.

As shown in Figure 4, the atomization rate of liquids with different viscosities shows a trend of increasing and then decreasing when the temperature changes from 30°C to 90°C, and it peaks at 40°C. The atomization rate decreases when the temperature is higher than 40°C, and the atomization rate drops to 0 when the temperature reaches 70°C. The experiment successfully proved the relationship between temperature and atomization rate. Meanwhile, according to Equation 21, it is known that the increase in the liquid temperature causes the decrease in the cavitation threshold, which in turn increases the cavitation intensity, resulting in the increase in the atomization rate. According to Equation 22, due to the increase in temperature, the cavitation nucleus collapses at a lower pressure, which causes the cavitation intensity to decrease, resulting in the decrease of the atomization rate.

The experiments showed that the lower cavitation thresholds increase the atomization rates, and lower collapse pressure reduces the atomization rate. At 40°C, the two factors of cavitation threshold and collapse pressure overlap each other to obtain the maximum atomization rate. Before the temperature reaches 40°C, the effect of a lower cavitation threshold is greater than that of a lower collapse pressure.

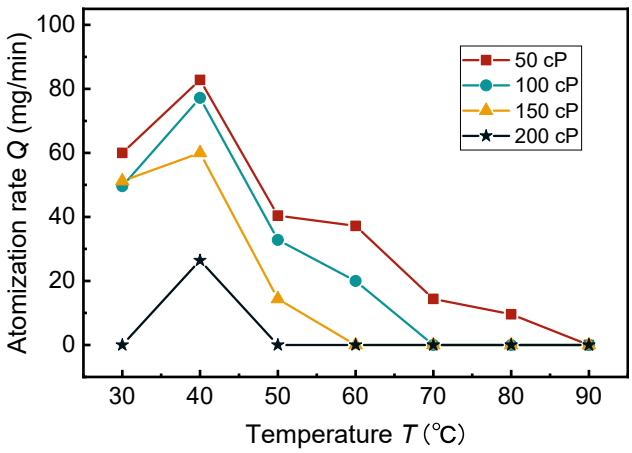

Figure 4. Relationship between atomization rate and temperature

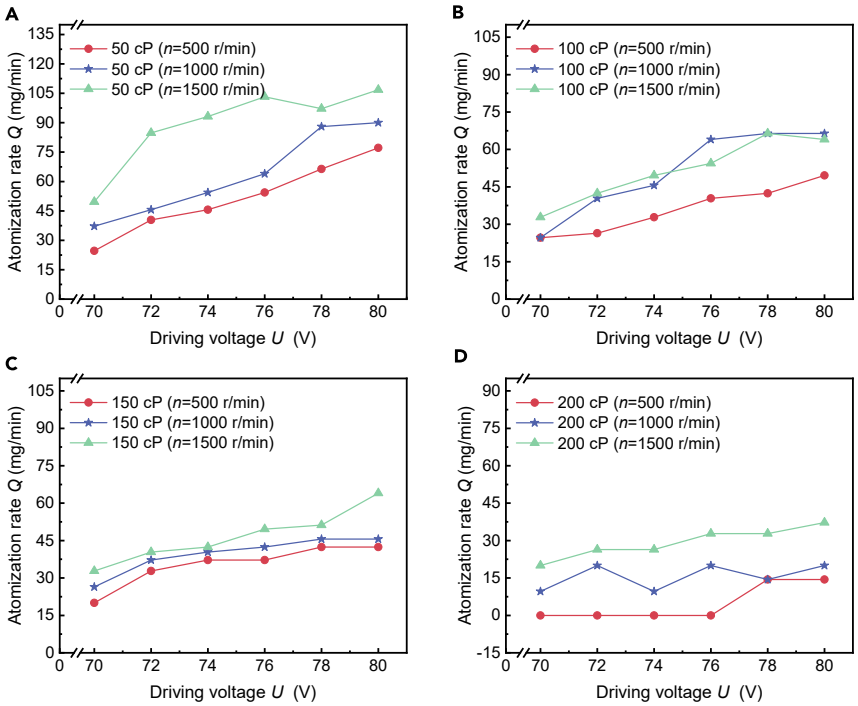

Figure 5. Relationship between stirring rate and atomization rate at different dynamic viscosities

(A) dynamic viscosity of 50 cP liquid.

(B) dynamic viscosity of 100 cP liquid.

(C) dynamic viscosity of 150 cP liquid.

(D) dynamic viscosity of 200 cP liquid.

Therefore, the atomization rate shows an increasing trend. After the temperature reaches 40°C, the effect of a lower cavitation threshold is weaker than that of a lower collapse pressure. Therefore, the atomization rate shows a decreasing trend. In conclusion, cavitation changes with temperature, which affects the atomization rate, and the atomization rate is positively correlated with cavitation. This experiment proves that cavitation is the determining mechanism of atomization.

Effect of stirring rate on atomization rate

The relationship between the stirring rate and atomization rate is shown in Figure 5, which shows the effect of the stirring rate on the atomization rate.

The trend of atomization rate with stirring rate is shown in Figure 5, and the change in atomization rate at different stirring rates for four different viscosity liquids is shown in Figures 5A–5D. The atomization rate increases with the rise in the stirring rate. The maximum atomization rate is 105 mg/min when the dynamic viscosity is 50 cP and the stirring rate is 1500 r/min. Analysis of temperature and stirring rate suggests that the number of bubbles increases with the rise in stirring rate. On the one hand, the cavitation threshold is lowered and cavitation is increased with the rise in the number of bubbles, and these phenomena achieve an increase in the atomization rate. On the other hand, the increase in the number of bubbles reduces the collapse pressure, which decreases cavitation to achieve a declined atomization rate. The changes in atomization rate caused by the cavitation threshold and the collapse pressure will intersect at a certain stirring rate. Similar to the temperature experiments, the atomization rate will tend to increase and then decrease in experiments where the stirring rate is the independent variable. However, the data in Figure 5 do not show a trend similar to the temperature experiment. Instead, the atomization rate continues to increase with the rise in the stirring rate. At stirring rates below 1500 r/min, the effect of the cavitation threshold change is greater than that of the cavitation intensity change. Therefore, the atomization rate shows an increasing trend after the two influencing factors are superimposed. This experimental result does not indicate a contradiction to theory, instead, the atomization rate will inflect at higher stirring rates. In conclusion, increasing the stirring rate to improve the gas content of the liquid and alter cavitation under the existing experimental conditions can change the atomization rate, and the atomization rate is positively correlated with cavitation. This experiment proves that cavitation is the determining mechanism of atomization.

The bubble density of the liquid at different stirring rates is shown in Figure 6, which shows the bubble distribution under the four groups of different stirring rates.

As shown in Figure 6, the observations from an ultradepth-of-field microscope were photographed, and the bubble density in the visual range was recorded. As shown in Figure 6A, no bubbles are observed in the visual range when the stirring rate is 0 r/min. As shown in

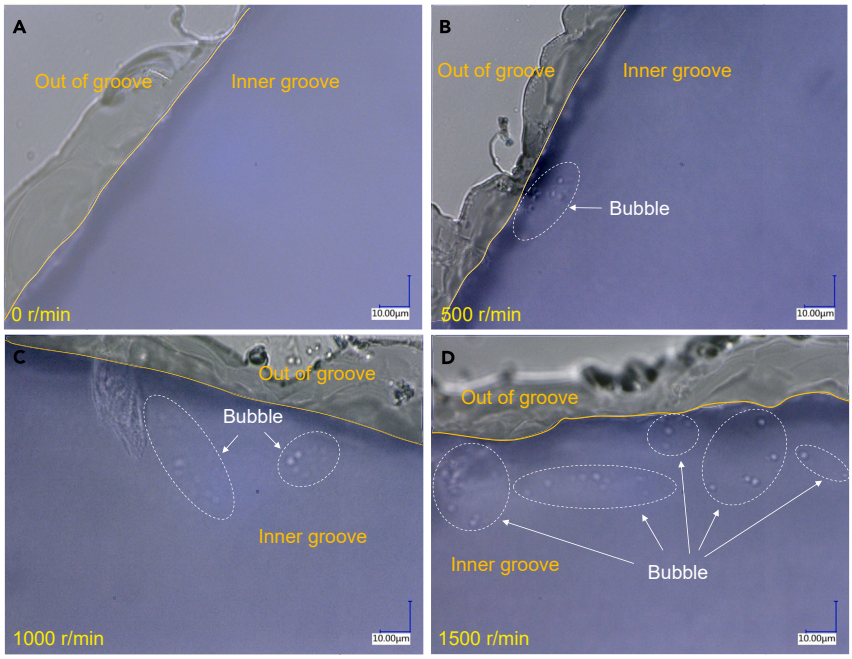

Figure 6. Bubble density of the liquid at different stirring rates

(A) 0 r/min.

(B) 500 r/min.

(C) 1000 r/min.

(D) 1500 r/min.

Figures 6B and 6C, bubbles appear in the visible range when stirring rates are 500 and 1000 r/min, and the bubble density increases with the rise in stirring rate. As shown in Figure 6D, the number of bubbles in the visible range increases when the stirring rate is 1500 r/min compared with the three other stirring rates. Therefore, observing the bubble density at different stirring rates in Figure 6 shows that the density of bubbles in the liquid increases with the rise in stirring rate, which proves that the probability of cavitation will become greater due to the increment in the number of bubbles. Thus, the atomization rate increases with the rise in stirring rate.

Results of Raman spectral analysis

The Raman spectral analysis of the liquids before and after atomization is shown in Figure 7, the position of the peak indicates the type of functional group and the height of the peak indicates the concentration of that functional group. The Raman spectra of the liquids before and after atomization at different temperatures are shown in Figures 7A–7B, the positions of the peaks of the Raman spectra for each temperature before and after atomization are at the same position, while the spectral peaks change in intensity, which shows that the chemical properties of the liquids before and after atomization at 30°C–45°C did not change, but the concentration of functional groups changes, which is due to the evaporation of water molecules in the liquids caused by heating, resulting in changes in the concentration of functional groups.

The Raman spectra of the liquids before and after atomization at different stirring rates are shown in Figures 7C and 7D, the positions of the peaks in the Raman spectra of the fluid at each stirring rate before and after atomization do not change, while the intensities of the peaks changes, it shows that the chemical properties of the liquids do not change before and after atomization at 0 r/min-1500 r/min, but rather the concentration of functional groups change, which is due to the incorporation of air during the mixing process, resulting in a change in the concentration of functional groups.

In conclusion, the experiments of Raman spectroscopy proved that the chemical properties of the liquids before and after atomization do not change because of the change of temperature at room temperature up to 45°C. Moreover, the chemical properties of the liquids before and after atomization do not change at a stirring rate of 1500 r/min. This demonstrates the safety of FTICA atomized products at optimal temperature (40°C) and optimal stirring rate (1500 r/min), and make FTICA better for biomedical applications.

Effect of temperature on atomized particles

The experimental results of the atomized particles test after the liquid has been heated are shown in Figure 8. The atomized particles of the fluids with a dynamic viscosity of 100 cP are normally distributed at the atomization temperatures of 25°C, 30°C, 35°C and 40°C, the average

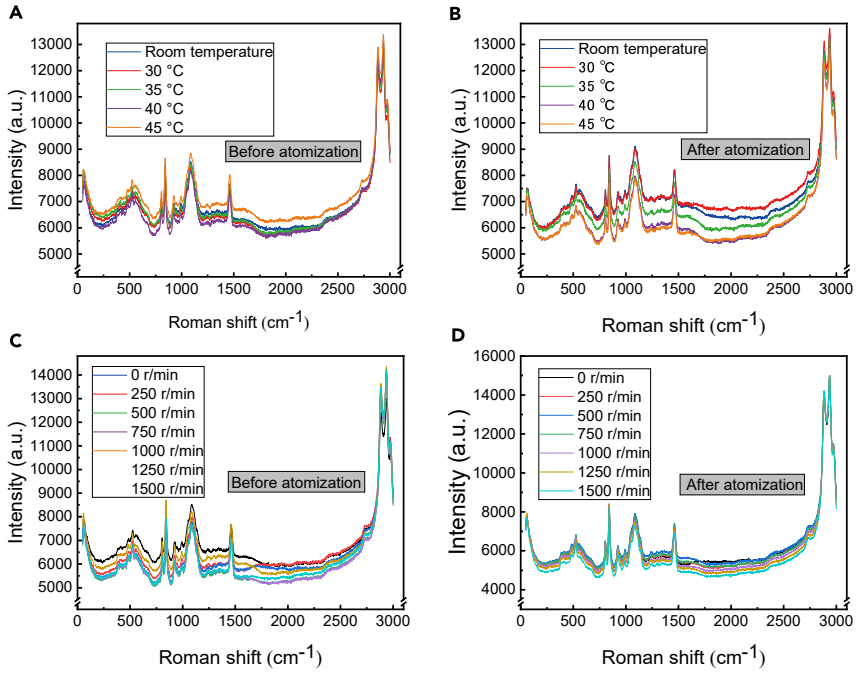

Figure 7. Results of Raman spectral analysis

(A) Raman spectra of the liquids before atomization at different temperatures.

(B) Raman spectra of the liquids after atomization at different temperatures.

(C) Raman spectra of liquids before atomization with different stirring rates.

(D) Raman spectra of liquids before atomization with different stirring rates.

diameters of the atomized particles were 13.742 μm, 12.879 μm, 13.338 μm, and 12.135 μm, respectively. The experimental results indicate that the average diameter of FTICA atomized particles varies between 12 μm and 14 μm at temperatures below 40°C, with no pattern of change observed as the temperature increases.

Effect of stirring rate on atomized particles

The experimental results of atomized particle testing after the liquid stirring treatment are shown in Figure 9. The atomized particles of the liquid with a dynamic viscosity of 100 cP were normally distributed at stirring rates of 0 r/min, 500 r/min, 1000 r/min, and 1500 r/min, the average diameters of the atomized particles were 12.485 μm, 12.095 μm, 12.803 μm, and 13.761 μm, respectively. From the experimental results, it can be obtained that the average diameter of the atomized particles of FTICA fluctuates in the range of 12 μm–14 μm below the stirring rate of 1500 r/min. There is no significant trend in the diameter of the atomized particles of FTICA as the stirring rate increases, which indicates that the change in stirring rate does not affect the atomized particles of FTICA below the stirring rate of 1500 r/min.

DISCUSSION

Theory of cavitation threshold

Cavitation theory suggests that any untreated liquid contains bubble nuclei (tiny bubbles). Liquid cavitation occurs after being excited by the force due to the existence of cavitation nuclei. The cavitation threshold for nucleated cavitation can be expressed as:[64]

$$P_B = P_0 - P_V + \frac{2}{3\sqrt{3}}\sqrt{\frac{\left(\frac{2\sigma}{R_0}\right)^3}{\left(P_0 - P_V + \frac{2\sigma}{R_0}\right)}}, \quad \text{(Equation 1)}$$

where P_0 is the environmental pressure, P_V is the saturated vapor pressure in the gas, σ is the surface tension coefficient, and R_0 is the radius of the cavitation nucleus.

The longitudinal and bending forces on the particle of the inner wall of the flow tube can be defined as follows[52]:

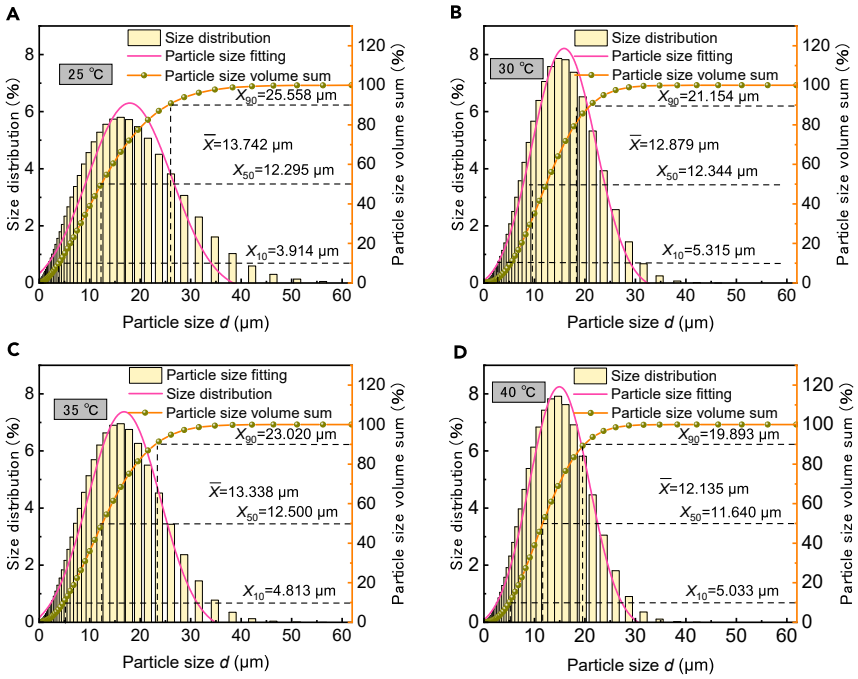

Figure 8. Results of atomized particles test after heating the liquid

(A) 25°C.

(B) 30°C.

(C) 35°C.

(D) 40°C.

$$\begin{cases} f_{u_1} = -\omega_0^2 m \dfrac{F\cos\theta e^{i\left(\omega_0 t-\varphi_{n_1}\right)} W_{n_1}(x_0) W_{n_1}(x)}{\left[K_{n_1}\sqrt{\left(1-\overline{\omega}_{n_1}^2\right)^2+\left(2\xi_{n_1}\overline{\omega}_{n_1}\right)^2}\right]} \\ f_{u_2} = -\omega_0^2 m \dfrac{F\sin\theta e^{i\left(\omega_0 t-\varphi_{n_2}\right)} W_{n_2}(x_0) W_{n_2}(x)}{\left[\overline{\omega}_{n_2}^2\sqrt{\left(1-\overline{\omega}_{n_2}^2\right)^2+\left(2\xi_{n_2}\overline{\omega}_{n_2}\right)^2}\right]} \end{cases}, \quad \text{(Equation 2)}$$

where f_{u_1} is the longitudinal force, f_{u_2} is the bending force, ω_0 is the excitation frequency, m is the mass of the particle, F is the amplitude of excitation force, θ is the tilt angle of the excitation force, φ_{n_1} is the phase of the longitudinal vibration, φ_{n_2} is the phase of the bending vibration, $W_{n_1}(x)$ is the longitudinal vibration mode at the horizontal coordinate point x, $W_{n_2}(x)$ is the bending vibration mode at the horizontal coordinate point x, x_0 is the action point of the excitation force in the horizontal coordinate, $\overline{\omega}_{n_1} = \frac{\omega_0}{\omega_{n_1}}$ is the ratio of longitudinal vibration excitation frequency to natural frequency, $\overline{\omega}_{n_2} = \frac{\omega_0}{\omega_{n_2}}$ is the ratio of longitudinal vibration excitation frequency to natural frequency bending vibration, K_{n_1} is the modal stiffness of longitudinal vibration, ξ_{n_1} is the relative damping coefficient of longitudinal vibration, and ξ_{n_2} is the relative damping coefficient of bending vibration.

The longitudinal and bending forces on the interior wall particle of the flow tube can be simplified as follows:

$$f_{u_1} = -\omega_0^2 m A_{n_1} e^{i\left(\omega_0 t-\varphi_{n_1}\right)} \quad \text{(Equation 3)}$$

$$f_{u_2} = -\omega_0^2 m A_{n_2} e^{i\left(\omega_0 t-\varphi_{n_2}\right)} \quad \text{(Equation 4)}$$

Cavitation nuclei are generated in the contact area between the inner wall of the flow tube and the liquid when the inner wall of the flow tube is vibrated by force. Therefore, the force on the single particle on the inner wall of the flow tube is approximated as the force on the bubble, that is, $P_{u_1} = f_{u_1}$, $P_{u_2} = f_{u_2}$. Then, combining the longitudinal and bending forces of Equation 2, the pressure on the cavitation nucleus can be expressed as:

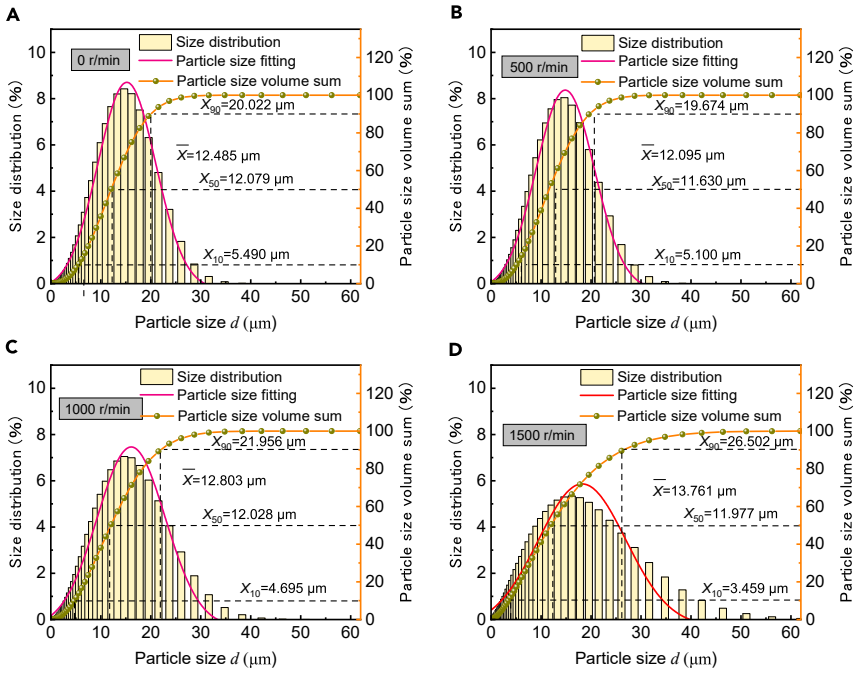

Figure 9. Results of atomized particles test after stirring the liquid

(A) 0 r/min.

(B) 500 r/min.

(C) 1000 r/min.

(D) 1500 r/min.

$$P_u = P_{u_1}\cos\left(\arctan\frac{P_{u_2}}{P_{u_1}}\right) = f_{u_1}^2\frac{1}{\sqrt{f_{u1}^2+f_{u_2}^2}}, \quad \text{(Equation 5)}$$

Therefore, combining Equations 3, 4, and 5, the cavitation nucleus force can be simplified as:

$$P_u = \frac{\omega_0^3 m A_{n_1}^2 e^{2i\left(\omega_0 t-\varphi_{n_1}\right)}}{\sqrt{A_{n_1}^2 e^{2i\left(\omega_0 t-\varphi_{n_1}\right)}+A_{n_2}^2 e^{2i\left(\omega_0 t-\varphi_{n_2}\right)}}} \quad \text{(Equation 6)}$$

where A_{n_1} is the longitudinal vibration amplitude of the excitation point at x_0, and A_{n_2} is the bending vibration amplitude of the excitation point at x_0. When the cavitation nucleus inside the liquid is excited by the above mentioned pressure P_u and pressure P_u is higher than the cavitation threshold P_B, cavitation occurs, and atomization is eventually achieved due to cavitation.

Multidimensional energy supply is the key to atomizing high-viscosity liquids. In this study, the liquid temperature and the liquid stirring rate (varying the number of bubbles) were varied to affect the cavitation from two different energy dimensions, and the atomization characteristic parameters were compared to study the relationship between cavitation and atomization.

Effect of cavitation

We analyzed the parameters that affect the cavitation threshold P_B and collapse pressure P_{max}, such as liquid viscosity η, surface tension coefficient σ, vapor pressure P_V, and the number of cavitation nuclei N, which will be beneficial in analyzing the effect of liquid temperature T and stirring rate n on cavitation.

The liquid viscosity η is a characterization of the interaction forces between molecules within the liquid. Therefore, for the cavitation effect inside the liquid, the internal molecular interaction forces are higher when the liquid viscosity η is higher, and therefore, the cavitation threshold P_B is higher. In the current study, an empirical equation was used to characterize the relationship between the liquid viscosity and the cavitation threshold:[52]

$$P_B = 0.8(\lg\eta + 5). \quad \text{(Equation 7)}$$

Therefore, the cavitation threshold P_B can be reduced by reducing the liquid viscosity η.

For the surface tension coefficient σ, transient cavitation theory[65] posits that the walls of the cavitation nucleus are excited by the force P_u, and the equation of motion can be expressed as:

$$R\left(\frac{d^2R}{dt^2}\right) + \frac{3}{2}\left(\frac{dR}{dt}\right)^2 = \frac{1}{\rho}\left(P_s - P_u - \frac{2\sigma}{R}\right), \quad \text{(Equation 8)}$$

where P_s is the expansion pressure in a cavitation nucleus of radius R, and P_s can be expressed as:

$$P_s = P_V + P_g\left(\frac{R_g}{R}\right)^3, \quad \text{(Equation 9)}$$

where P_g is the pressure in the cavitation nucleus with initial radius R_g. By ignoring the surface tension of the cavitation nucleus and the vapor pressure inside the cavitation nucleus, R_g is replaced by R_m, that is, $\frac{2\sigma}{R} = 0$, $P_V = 0$, $R_m = R_g$, and the cavitation nuclear collapse is considered to be an adiabatic process. Consequently, Equation 8 can be expressed as:

$$R\left(\frac{d^2R}{dt^2}\right) + \frac{3}{2}\left(\frac{dR}{dt}\right)^2 = \frac{1}{\rho}\left[P_g\left(\frac{R_m}{R}\right)^{3\gamma} - P_u\right], \quad \text{(Equation 10)}$$

where R_m is the radius at which the cavitation nucleus starts to collapse, and $\gamma = \frac{C_p}{C_V}$ is the ratio of specific heat at constant pressure to specific heat at constant volume.

The radius of the cavitation nucleus is compressed to a minimum value R_{min} when the acoustic pressure is positive, and the radius of the cavitation nucleus begins to expand to the collapse radius R_m when the acoustic pressure is negative. The size of the bubble varies between R_{min} and R_m. When the cavitation nucleus wall moves to the two extreme points of R_{min} and R_m, the velocity is 0, that is, $\frac{dR}{dt} = 0$. To determine the radius of the cavitation nucleus, the integral of Equation 7 needs to be determined by

$$P_u(Z-1)(\gamma-1) = P_g(Z^\gamma - Z), \quad \text{(Equation 11)}$$

where $\left(\frac{R_m}{R}\right)^3 = Z$ and $\frac{dR}{dt} = 0$. Given that (Z-1) is approximated by Z when R is quite small, Equation 11 can be expressed as

$$Z = \left[\frac{P_u(\gamma-1)}{P_g}\right]^{\frac{1}{\gamma-1}}. \quad \text{(Equation 12)}$$

When the cavitation nucleus takes the minimum volume V_{min}, the pressure in the cavitation nucleus reaches a collapse value P_{max}, and the following relationship can be expressed as[66]:

$$P_{max}V_{min}^\gamma = P_gV_{max}^\gamma, \quad \text{(Equation 13)}$$

where $P_g = P_{min}$ and $\gamma = \frac{C_p}{C_V}$ is the ratio of specific heat at constant pressure to specific heat at constant volume.

Given that the relationship between the volume V of the cavitation nucleus and the radius R of the cavitation nucleus is $V = \frac{4}{3}\pi R^3$, the following can be obtained

$$\frac{V_{max}}{V_{min}} = \left(\frac{R_m}{R_{min}}\right)^3 = Z, \quad \text{(Equation 14)}$$

according to Equations 12 and 13, the following can be obtained

$$\left(\frac{V_{max}}{V_{min}}\right)^\gamma = \frac{P_{max}}{P_g} = Z^\gamma, \quad \text{(Equation 15)}$$

according to Equations 12 and 15, the collapse pressure P_{max} of the cavitation nucleus can be expressed as

$$P_{max} = P_g\left[\frac{P_u(\gamma-1)}{P_g}\right]^{\frac{\gamma}{\gamma-1}}. \quad \text{(Equation 16)}$$

The specific heat capacity ratio γ is assumed to be constant at 1.33 to study the effect of vapor pressure P_V on cavitation. Therefore, the collapse pressure P_{max} in the cavitation nucleus is proportional to:[65]

$$P_{max} \sim P_u^4P_g^{-3}. \quad \text{(Equation 17)}$$

In acoustic chemistry applications, the bubble pressure P_g is taken as the liquid vapor pressure P_V, and thus the relationship between the cavitation nucleus collapse pressure and the liquid vapor pressure can be expressed as:

$$P_{max} \sim P_u^4P_V^{-3}. \quad \text{(Equation 18)}$$

The liquid viscosity and vapor pressure as a function of temperature can be expressed as follows[67,68]:

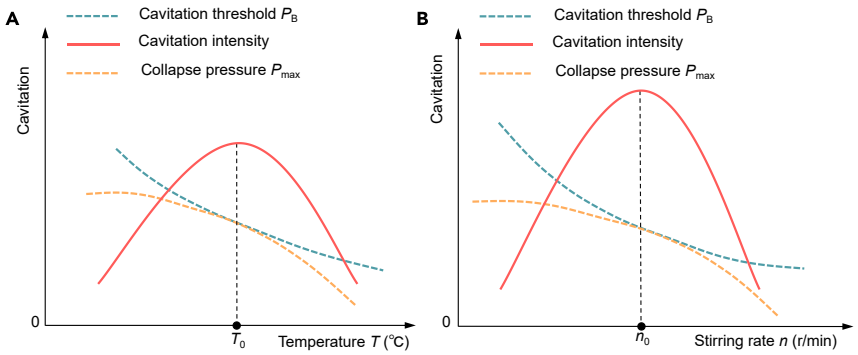

Figure 10. Effect of cavitation parameters on cavitation

(A) relationship between temperature and cavitation.

(B) relationship between stirring rate and cavitation.

$$\eta = \eta_0[1 + B(T - T_0)] \quad \text{(Equation 19)}$$

$$\lg P_V = A - \frac{B}{C+T} \quad \text{(Equation 20)}$$

Where η_0 is the viscosity of the fluid at the reference temperature T_0. B is the temperature coefficient, T is the absolute temperature of the liquid. A, B, and C are the coefficients of the regression.

Combining Equations 7 and 19, the relationship between cavitation threshold and liquid temperature can be expressed as:

$$P_B = 0.8 \lg[\eta_0 + \eta_0 B(T - T_0)] + 4 \quad \text{(Equation 21)}$$

Combining Equations 18 and 20, the relationship between the collapse pressure of the cavitation nucleus and the liquid temperature can be expressed as:

$$P_{max} \sim 10^{-3\left(A - \frac{B}{C+T}\right)} P_u^4. \quad \text{(Equation 22)}$$

The flow tube of FTICA generates periodic vibration when subjected to an excitation force, and when the cavitation nucleus is subjected to an external force P_u larger than the cavitation threshold P_B under the steady state response, the cavitation effect occurs in the liquid of the inner wall of the flow tube. The cavitation nucleus absorbs energy in an extremely short period of time, contracting and expanding in response to positive and negative changes in pressure amplitude. The cavitation nucleus volume contraction to a minimum when the collapse, and in the collapse of the instantaneous generation of a strong instantaneous collapse pressure P_{max} effect on the liquid to achieve atomization. The cavitation nucleus collapse pressure P_{max} is the directly responsible for the atomization of high-viscosity liquids in this study. Therefore, the lower the cavitation threshold P_B, the more likely cavitation occurs, and the greater the atomization rate, the higher the cavitation core collapse pressure P_{max}, the higher the atomization rate. It can be obtained from Equation 21 that the cavitation threshold decreases with increasing liquid temperature. From Equation 22, it can be obtained that the collapse pressure of the cavitation nucleus decreases with increasing liquid temperature.

In studying the effect of the bubble number N on cavitation, Equation 1 shows that the increase in the number of bubbles N causes more weak points inside the liquid, the cavitation threshold P_B also decreases, and then cavitation is more likely to occur. However, the continuous increase in the number of bubbles N causes an increase in vapor pressure P_V and cavitation nucleus pressure P_g. Eventually, the collapse pressure P_{max} decreases and the cavitation intensity decreases.

Analysis of temperature and stirring rate

In this study, the abovementioned parameters were varied by changing two conditions, namely, the temperature and the stirring rate, to change the cavitation. Finally, the relationship between cavitation and atomization rate was discussed. If the cavitation is positively correlated with the atomization rate, then cavitation is the determining mechanism for the atomization of high-viscosity liquid. Otherwise, cavitation does not determine atomization. The atomization of high-viscosity liquid is caused by the energy provided by multidimensional vibrations, and cavitation is a concomitant phenomenon in the atomization process. The effect of cavitation parameters on cavitation is shown in Figure 10.

First, the temperature has an effect on several cavitation parameters. According to Equations 21 and 22, with the temperature increases, on the one hand, the cavitation threshold is lowered, which increases the cavitation; on the other hand, with the increase of temperature, the collapse pressure decreases, which leads to the decrease of cavitation. The study by Niemczewski showed that the increase in temperature causes a bidirectional change in cavitation, and the cavitation intensity shows a trend of increasing and then decreasing with the continuous

rise in temperature.[69] On this basis, we will explore the effect of temperature-induced changes in cavitation on atomization efficiency. Therefore, the bidirectional effects of cavitation threshold and collapse pressure on atomization need to be considered to discuss the relationship between cavitation and atomization rate.

Second, the stirring rate mainly affects the number of bubbles. During the process of stirring the liquid, the shear force of the rotor rotation disperses the liquid into numerous liquid clusters of different sizes. These liquid clusters increase the chance of contact with air under the action of a vortex, which raises the total contact area between the liquid and air. This condition allows more bubbles to be dissolved in the liquid. Consequently, the stirring rate is proportional to the number of bubbles. The abovementioned study shows that, with the rise in the number of cavitation nuclei, the probability of cavitation will increase, which will lead to a lower cavitation threshold and thus increase cavitation. Meanwhile, some of the defective bubbles cavitate first in the process of high-frequency vibration because of the excessive number of bubbles. Part of the energy generated by the cavitation of these bubbles will also be absorbed by other bubbles that have not cavitated. In this way, the collapse pressure is reduced, which leads to lower cavitation. On this basis, we investigate the effect of cavitation changes caused by air content on atomization efficiency. Similar to the effect of temperature, we need to consider the bidirectional effects of the cavitation threshold and collapse pressure on atomization at the liquid stirring rate to discuss the relationship between cavitation and atomization rate.

Conclusion

Cavitation is proven to be a decisive mechanism for the atomization of high-viscosity liquids, in contrast to the widely supported capillary wave hypothesis, our study provides evidence in favor of the cavitation hypothesis. At the same time, the optimal atomization conditions of the FTICA were studied to explore the possibility of application in the field of biotherapeutics. First, the effects of liquid viscosity, surface tension of gas inside the liquid, saturated vapor pressure, and the number of bubbles on the cavitation threshold and collapse pressure were analyzed theoretically. Then, the effect of the change in cavitation on the atomization rate was obtained. On the basis of the theoretical analysis, temperature and stirring experiments were next conducted to verify the effect of cavitation on the atomization rate. The following conclusions were obtained.

(1) The atomization rate is proven to be positively correlated with cavitation, and cavitation is the determining factor for the atomization of high-viscosity liquids, which verifies the correctness of the cavitation hypothesis.
(2) The optimal atomization temperature of the liquids is about 40°C, which is suitable for the effective atomization of biological proteins and other medicinal liquids.
(3) The Raman spectroscopy experiments proved that the chemical properties of the products before and after atomization did not change when the liquid was at a temperature of 40°C and a stirring rate of 1500 r/min, indicating the safety of FTICA for biomedical applications.
(4) Experiments have shown that an appropriate increase in temperature and stirring rate can increase the atomization rate of a liquid with the same viscosity, and it raises the liquid dynamic viscosity of atomization to 200 cP.

In this study, we prove that cavitation is the decisive mechanism for the atomization of high-viscosity liquid by changing the physical properties of the liquid. Therefore, FTICA can respond to applications in genetic engineering, fuel supply, and microfabrication technology. This study provides an important reference for future research on the ultrasonic atomization of high-viscosity liquids and is beneficial to explore the range of applications for the atomization of high-viscosity liquid.

Limitations of the study

While this study indirectly verifies the cavitation effect of FTICA, it is limited by the cavitation effect detection method, and due to the small inner diameter of the flow tube, it is difficult for existing techniques to directly detect the cavitation effect inside the atomized flow tube. Therefore, in the subsequent research, we can try to design the experimental method to directly detect the cavitation effect of the flow tube type atomizer.

STAR★METHODS

Detailed methods are provided in the online version of this paper and include the following:

- KEY RESOURCES TABLE
- RESOURCE AVAILABILITY
  - Lead contact
  - Materials availability
  - Data and code availability
- METHOD DETAILS
  - Structure of the FTICA
- EXPERIMENTAL MODEL AND SUBJECT DETAILS
  - Impedance measurement experiment
  - Experiments of viscosity analysis

- Experiment of temperature and atomization rate
- Experiment of temperature and stirring rate
- Experiment of Raman spectral analysis
- Experiments on the relationship between temperature and atomized particles
- Experiments on the relationship between stirring and atomized particles

ACKNOWLEDGMENTS

This work was supported by Guangdong Basic and Applied Basic Research Foundation (Grant No. 2022A1515010265 and 2020A1515110619), Science and Technology Program of Guangzhou (Grant No. 202201020158), Science and Technology Planning Project of Guangzhou City (Grant No. 2023A03J0120), Science and Technology Program of Guangzhou City Joint with Universities (Grant No. 202201020191), On campus research projects at Guangzhou University (Grant No. ZH2023002), R&D Program of Joint Institute of GZHU & ICoST (Grant No. GI202108), The Graduate-Ability-Promotion Plan of Guangzhou University (Granted No. 2022GDJC-M21).

AUTHOR CONTRIBUTIONS

Z. Z. Gui: Methodology, investigation, and writing-original draft. Y. H. Zeng: Methodology, formal analysis, and writing-original draft. T. Xie: Formal analysis and writing-original draft. B. C Chen: Investigation. J. L. Wang: Investigation. Y. X. Wen: Validation. T. Tan: Investigation. T. Zou: Conceptualization and methodology. F. Zhang: Formal analysis and writing-review and editing. J. H. Zhang: Conceptualization, methodology, and supervision.

DECLARATION OF INTERESTS

The authors declare that they have no known competing financial interests or personal relationships that could have appeared to influence the work reported in this article.

Received: November 1, 2023
Revised: March 13, 2024
Accepted: May 17, 2024
Published: May 22, 2024

REFERENCES

1. Stepien, Z., Pielecha, I., Szwajca, F., and Cieslik, W. (2022). Effects of Ethanol Admixtures with Gasoline on Fuel Atomization Characteristics Using High-Pressure Injectors. Energies *15*, 2926. https://doi.org/10.3390/en15082926.
2. Bianchi, G.M., Pelloni, P., Corcione, F.E., Allocca, L., and Luppino, F. (2001). Modeling atomization of high-pressure diesel sprays. J. Eng. Gas Turbine. Power *123*, 419–427. https://doi.org/10.1115/1.1361110.
3. Wittner, M., Karbstein, H., and Gaukel, V. (2019). Air-core-liquid-ring (aclr) atomization: influences of gas pressure and atomizer scale up on atomization efficiency. Processes *7*, 139. https://doi.org/10.3390/pr7030139.
4. Mao, X., Xie, Q., Duan, Y., Yu, S., Liang, X., Wu, Z., Lu, M., and Nie, Y. (2020). Predictive models for characterizing the atomization process in pyrolysis of methyl ricinoleate. Chin. J. Chem. Eng. *28*, 1023–1028. https://doi.org/10.1016/j.cjche.2020.02.007.
5. Jia, J., Zhao, L., Liu, Z., Hao, X., Huo, L., Zhao, Y., and Yao, Z. (2022). Spray atomization characteristics of biomass pyrolysis tar: influence of methanol addition, temperature, and atomization pressure. Energy *242*, 122534. https://doi.org/10.1016/j.energy.2021.122534.
6. Liu, S., Lin, R., Li, Z., Ying, C., and Kang, Y. (2017). Experimental research on atomization parameters in spray cooling system. In 20th International Conference on Electrical Machines and Systems (ICEMS), pp. 1–5. https://doi.org/10.1109/ICEMS.2017.8056328.
7. Qu, S., Zhang, C., Liang, Y., Ma, Z., Meng, F., Wang, Z., Xu, P., Yu, T., and Zhao, J. (2022). Experimental investigation of ultrasonic-vibration polishing of k9 optical glass based on ultrasonic atomization. Ceram. Int. *48*, 9067–9074. https://doi.org/10.1016/j.ceramint.2021.12.090.
8. Zhang, Y., Yuan, S., and Gao, Y. (2023). Spatial distribution and transient evolution of sub-droplet velocity and size in ultrasonic atomization. Exp. Therm. Fluid Sci. *140*, 110761. https://doi.org/10.1016/j.expthermflusci.2022.110761.
9. Dalmoro, A., Barba, A.A., Lamberti, G., and d'Amore, M. (2012). Intensifying the microencapsulation process: Ultrasonic atomization as an innovative approach. Eur. J. Pharm. Biopharm. *80*, 471–477. https://doi.org/10.1016/j.ejpb.2012.01.006.
10. Sung, C.C., Bai, C.Y., Chang, S.J., and Chen, J.H. (2012). Controllable fuel cell humidification by ultrasonic atomization. J. Acoust. Soc. Am. *131*, 3526. https://doi.org/10.1121/1.4709337.
11. Wang, Y., and Wakisaka, M. (2015). Chitosan nanofibers fabricated by combined ultrasonic atomization and freeze casting. Carbohydr. Polym. *122*, 18–25. https://doi.org/10.1016/j.carbpol.2014.12.080.
12. Khaire, R.A., and Gogate, P.R. (2021). Novel approaches based on ultrasound for spray drying of food and bioactive compounds. Technol. *3*, 1832–1853. https://doi.org/10.1080/07373937.2020.1804926.
13. Chang, W.C., Lan, D.H., Lee, K.M., Wang, X.F., and Liu, C.L. (2017). Controlled deposition and performance optimization of perovskite solar cells using ultrasonic spray-coating of photoactive layers. ChemSusChem *10*, 1405–1412. https://doi.org/10.1002/cssc.201601711.
14. Park, S., and Park, K. (2022). Principles and droplet size distributions of various spraying methods: A review. J. Mech. Sci. Technol. *36*, 4033–4041. https://doi.org/10.1007/s12206-022-0724-3.
15. Samuel, J., and Smaldone, G.C. (2020). Maximizing deep lung deposition in healthy and fibrotic subjects during jet nebulization. J. Aerosol Med. Pulm. Drug Deliv. *33*, 108–115. https://doi.org/10.1089/jamp.2019.1552.
16. Zhang, H., Wu, Y., Wan, X., Shen, Y., Le, Q., Yang, P., Zhou, S., Zhou, X., Zhou, F., Gu, H., and Hong, J. (2023). Effect of Hypochlorous Acid on Blepharitis through Ultrasonic Atomization: A Randomized Clinical Trial. J. Clin. Med. *12*, 1164.
17. Arita, R., Morishige, N., Shirakawa, R., Sato, Y., and Amano, S. (2015). Effects of eyelid warming devices on tear film parameters in normal subjects and patients with meibomian gland dysfunction. Ocul. Surf. *13*, 321–330. https://doi.org/10.1016/j.jtos.2015.04.005.
18. Huang, W.T., Chou, F.I., Tsai, J.T., and Chou, J.H. (2020). Application of graphene nanofluid/ultrasonic atomization MQL system in micromilling and development of optimal predictive model for SKH-9 high-speed steel using fuzzy-logic-based multi-objective design. Int. J. Fuzzy Syst. *22*, 2101–

2118. https://doi.org/10.1007/s40815-020-00930-w.
19. Hu, Y., Meng, J., Hu, Z., Zhou, H., Luan, X., Huang, B., and Wei, X. (2021). Machining characteristics of Ti 6 Al 4 V alloy turning assisted by laser heating and ultrasonic atomization. Appl. Opt. *60*, 2583–2590. https://doi.org/10.1364/AO.418023.
20. Zheng, J., Tang, G., Su, F., Li, T., Liang, Z., and Liu, X. (2023). Facile fabrication of aluminium alloys with gradient nanostructures incorporating α-Al2O3 particles for enhanced tribological properties. Tribol. Int. *189*, 108921. https://doi.org/10.1016/j.triboint.2023.108921.
21. Tang, G., Su, F., Liu, X., Liang, Z., Zou, T., and Chu, P.K. (2023). Origin of superlubricity promoted by black phosphorus dotted with gold nanoparticles. Appl. Surf. Sci. *613*, 156030. https://doi.org/10.1016/j.apsusc.2022.156030.
22. Zhao, Q., Xie, M., Liu, Y., and Yi, J. (2017). Improved electroless plating method through ultrasonic spray atomization for depositing silver nanoparticles on multi-walled carbon nanotubes. Appl. Surf. Sci. *409*, 164–168. https://doi.org/10.1016/j.apsusc.2017.03.032.
23. Komatsu, N. (2009). Novel and practical separation processes for fullerenes, carbon nanotubes and nanodiamonds. J. Jpn. Petrol. Inst. *52*, 73–80. https://doi.org/10.1627/jpi.52.73.
24. Li, Y., Liu, Z., He, Z., Tu, L., and Huang, H.Z. (2023). Fatigue reliability analysis and assessment of offshore wind turbine blade adhesive bonding under the coupling effects of multiple environmental stresses. Reliab. Eng. Syst. Saf. *238*, 109426. https://doi.org/10.1016/j.ress.2023.109426.
25. Eslamian, M. (2013). A mathematical model for the design and fabrication of polymer solar cells by spray coating. Dry. Technol. *31*, 405–413. https://doi.org/10.1080/07373937.2012.737397.
26. Park, H.W., Choi, S., and Park, D.W. (2015). Simultaneous treatment of NO and SO2 with aqueous NaClO2 solution in a wet scrubber combined with a plasma electrostatic precipitator. J. Hazard Mater. *285*, 117–126. https://doi.org/10.1016/j.jhazmat.2014.11.040.
27. Park, H.W., and Park, D.W. (2017). Removal kinetics for gaseous NO and SO2 by an aqueous NaClO2 solution mist in a wet electrostatic precipitator. Environ. Technol. *38*, 835–843. https://doi.org/10.1080/09593330.2016.1213770.
28. Han, Z., Zhao, D., Zheng, D., Pan, X., Liu, B., Han, Z., Gao, Y., Wang, J., and Yan, Z. (2018). No removal from simulated flue gas with a naclo2 mist generated using the ultrasonic atomization method. Energies *11*, 1043.
29. Elsa, B.M., Alexie, M., Laurent, V., Renaud, R., and Heuzé-Vourc'h, N. (2018). Designing inhaled protein therapeutics for topical lung delivery: what are the next steps? Expert Opin. Drug Deliv. *15*, 729–736. https://doi.org/10.1080/17425247.2018.1503251.
30. Kaur, R., Garg, T., Rath, G., and Goyal, A.K. (2014). Advanced aerosol delivery devices for potential cure of acute and chronic diseases. Crit. Rev. Ther. Drug Carrier Syst. *31*, 495–530. https://doi.org/10.1615/CritRevTherDrugCarrierSyst.2014010527.
31. Andrade Almeida, P.C., Smith, K., Hearson, G., Martin, M.J., and Harrison, T.W. (2022). Comparing ultrasonic and breath-actuated jet nebulisers for sputum induction. Eur. Respir. J. *60*, 368. https://doi.org/10.1183/13993003.congress-2022.368.
32. Khan, I., Hussein, S., Houacine, C., Khan Sadozai, S., Islam, Y., Bnyan, R., Elhissi, A., and Yousaf, S. (2021). Fabrication, characterization and optimization of nanostructured lipid carrier formulations using Beclomethasone dipropionate for pulmonary drug delivery via medical nebulizers. Int. J. Pharm. *598*, 120376. https://doi.org/10.1016/j.ijpharm.2021.120376.
33. Lu, Q., Yang, J., Liu, Z., Gutierrez, C., Aymard, G., and Rouby, J.J.; Nebulized Antibiotics Study Group (2011). Nebulized ceftazidime and amikacin in ventilator-associated pneumonia caused by Pseudomonas aeruginosa. Am. J. Resp. Crit. Care *184*, 106–115. https://doi.org/10.1164/rccm.201011-1894OC.
34. Li, B., Wang, W., Song, W., Zhao, Z., Tan, Q., Zhao, Z., Tang, L., Zhu, T., Yin, J., Bai, J., et al. (2021). Antiviral and Anti-Inflammatory Treatment with Multifunctional Alveolar Macrophage-Like Nanoparticles in a Surrogate Mouse Model of COVID-19. Adv. Sci. *8*, 2003556. https://doi.org/10.1002/advs.202003556.
35. Lehmann, J., Agel, M.R., Engelhardt, K.H., Pinnapireddy, S.R., Agel, S., Duse, L., Preis, E., Wojcik, M., and Bakowsky, U. (2021). Improvement of pulmonary photodynamic therapy: nebulisation of curcumin-loaded tetraether liposomes. Pharmaceutics *13*, 1243.
36. Szabová, J., Mišík, O., Fučík, J., Mrázová, K., Mravcová, L., Elcner, J., Lízal, F., Krzyžánek, V., and Mravec, F. (2023). Liposomal form of erlotinib for local inhalation administration and efficiency of its transport to the lungs. Int. J. Pharm. *634*, 122695. https://doi.org/10.1016/j.ijpharm.2023.122695.
37. Said-Elbahr, R., Nasr, M., Alhnan, M.A., Taha, I., and Sammour, O. (2022). Simultaneous pulmonary administration of celecoxib and naringin using a nebulization-friendly nanoemulsion: A device-targeted delivery for treatment of lung cancer. Expert Opin. Drug Deliv. *19*, 611–622. https://doi.org/10.1080/17425247.2022.2076833.
38. Xu, L., Liu, M.Z., Yang, Y.Y., Wang, Y., Hua, X.X., Du, L.X., Zhu, J.Y., Shen, Y., Wang, Y.Q., Zhang, L., et al. (2022). Geraniol enhances inhibitory inputs to the paraventricular thalamic nucleus and induces sedation in mice. Phytomedicine *98*, 153965. https://doi.org/10.1016/j.phymed.2022.153965.
39. Dehingia, K., Sarmah, H.K., Das, A., Park, C., and Hosseini, K. (2022). A STUDY ON A GENE THERAPY MODEL FOR THE COMBINED TREATMENT OF CANCER, Eurasian J. Math. Comp. Appl. *10*, 15–36. https://doi.org/10.32523/2306-6172-2022-10-3-15-36.
40. Shimamura, M., Nakagami, H., Sanada, F., and Morishita, R. (2020). Progress of gene therapy in cardiovascular disease. Hypertension *76*, 1038–1044. https://doi.org/10.1161/HYPERTENSIONAHA.120.14478.
41. Hu, Y.F., Fang, Y.H., Lai, Y.R., Feng, X.Q., and Xu, S.Q. (2022). Application of Gene Therapy in Hemophilia. Curr. Med. Sci. *42*, 925–931. https://doi.org/10.1007/s11596-022-2645-x.
42. Christakopoulos, G.E., Telange, R., Yen, J., and Weiss, M.J. (2023). Gene Therapy and Gene Editing for β-Thalassemia. Hematol. Oncol. Clin. North Am. *37*, 433–447. https://doi.org/10.1016/j.hoc.2022.12.012.
43. Kuo, C.Y., and Kohn, D.B. (2020). Overview of the current status of gene therapy for primary immune deficiencies (PIDs). J. Allergy Clin. Immunol. *146*, 229–233. https://doi.org/10.1016/j.jaci.2020.05.024.
44. Akinc, A., Maier, M.A., Manoharan, M., Fitzgerald, K., Jayaraman, M., Barros, S., Ansell, S., Du, X., Hope, M.J., Madden, T.D., et al. (2019). The Onpattro story and the clinical translation of nanomedicines containing nucleic acid-based drugs. Nat. Nanotechnol. *14*, 1084–1087. https://doi.org/10.1038/s41565-019-0591-y.
45. Rotolo, L., Vanover, D., Bruno, N.C., Peck, H.E., Zurla, C., Murray, J., Noel, R.K., O'Farrell, L., Araínga, M., Orr-Burks, N., et al. (2023). Species-agnostic polymeric formulations for inhalable messenger RNA delivery to the lung. Nat. Mater. *22*, 369–379. https://doi.org/10.1038/s41563-022-01404-0.
46. Elia, U., Kon, E., and Peer, D. (2023). CRISPR editing in the lung with novel lipids. Nat. Biotechnol. *41*, 1387–1388. https://doi.org/10.1038/s41587-023-01744-5.
47. Mc Callion, O.N.M., and Patel, M.J. (1996). Viscosity effects on nebulisation of aqueous solutions. Int. J. Pharm. X. *130*, 245–249. https://doi.org/10.1016/0378-5173(95)04291-1.
48. Finlay, W.H., Lange, C.F., King, M., and Speert, D.P. (2000). Lung delivery of aerosolized dextran. Crit. Care *161*, 91–97. https://doi.org/10.1164/ajrccm.161.1.9812094.
49. Beck-Broichsitter, M. (2019). Making concentrated antibody formulations accessible for vibrating-mesh nebulization. J. Pharm. Sci. *108*, 2588–2592. https://doi.org/10.1016/j.xphs.2019.03.009.
50. Law, J., Kong, K.W., Chan, H.Y., Sun, W., Li, W.J., Chau, E.B.F., and Chan, G.K.M. (2017). Atomization of High-Viscosity Fluids for Aromatherapy Using Micro-heaters for Heterogeneous Bubble Nucleation. Sci. Rep. *7*, 40289. https://doi.org/10.1038/srep40289.
51. Vermeer, A.W., Bremer, M.G., and Norde, W. (1998). Structural changes of IgG induced by heat treatment and by adsorption onto a hydrophobic Teflon surface studied by circular dichroism spectroscopy. BBA-Gen Subjects *1425*, 1–12. https://doi.org/10.1016/S0304-4165(98)00048-8.
52. Xie, T., Zeng, Y., Gui, Z., Ma, M., Huo, Y., Zhang, W., Tan, T., Zou, T., Zhang, F., and Zhang, J. (2023). Piezoelectric atomization of liquids with dynamic viscosities up to 175 cP at room temperature. Ultrason. Sonochem. *94*, 106331. https://doi.org/10.1016/j.ultsonch.2023.106331.
53. Kannan, Y.S., Karri, B., and Sahu, K.C. (2018). Letter: Entrapment and interaction of an air bubble with an oscillating cavitation bubble. Phys. Fluids *30*. https://doi.org/10.1063/1.5025122.
54. Kannan, Y.S., Balusamy, S., Karri, B., and Sahu, K.C. (2020). Effect of viscosity on the volumetric oscillations of a non-equilibrium bubble in free-field and near a free-surface. Fluid Sci. *116*, 110113. https://doi.org/10.1016/j.expthermflusci.2020.110113.
55. Rajan, R., and Pandit, A.B. (2001). Correlations to predict droplet size in ultrasonic atomisation. Ultrasonics *39*, 235–255. https://doi.org/10.1016/S0041-624X(01)00054-3.
56. Taylor, G.I. (1950). The instability of liquid surfaces when accelerated in a direction perpendicular to their planes. I. Proc. R. Soc. Lon. Ser. A: Math. Phy. Sci. *201*, 192–196. https://doi.org/10.1098/rspa.1950.0052.
57. Galleguillos, R. (2022). Acoustic cavitation detection during ultrasonic atomization

process. Appl. Acoust. *192*, 108716. https://doi.org/10.1016/j.apacoust.2022.108716.
58. Boguslavski, Y.Y. (1969). Physical mechanism of the acoustic atomization of a liquid. Sov. Phys. Acoust. *15*, 14–21. https://doi.org/10.1016/0041-624x(70)90819-x.
59. Topp, M.N. (1973). Ultrasonic atomization-a photographic study of the mechanism of disintegration. J. Aerosol Sci. *4*, 17–25. https://doi.org/10.1016/0021-8502(73)90113-4.
60. Friend, J., and Yeo, L.Y. (2011). Microscale acoustofluidics: Microfluidics driven via acoustics and ultrasonics. Rev. Mod. Phys. *83*, 647–704. https://doi.org/10.1103/RevModPhys.83.647.
61. Cai, Y., Zhang, J., Zhu, C., Huang, J., and Jiang, F. (2016). Theoretical calculations and experimental verification for the pumping effect caused by the dynamic micro-tapered angle. Chin. J. Mech. Eng. *29*, 615–623. https://doi.org/10.3901/CJME.2016.0324.037.
62. Yan, Q., Zhang, J., Huang, J., and Wang, Y. (2018). The effect of vibration characteristics on the atomization rate in a micro-tapered aperture atomizer. Sensors *18*, 934.
63. Yan, Q., Sun, W., and Zhang, J. (2020). Study on the influencing factors of the atomization rate in a piezoceramic vibrating mesh atomizer. Appl. Sci. *10*, 2422.
64. Fujikawa, T., Egashira, R., Hooman, K., Yaguchi, H., Masubuchi, H., and Fujikawa, S. (2022). Theory of dynamical cavitation threshold for diesel fuel atomization. Fluid Dyn. Res. *54*, 045505. https://doi.org/10.1088/1873-7005/ac830d.
65. Feng, N., and Li, H. (1992). Sonochemistry and its Application (Anhui Science & Technology Publishing House).
66. Yi, J., and Lu, Y. (2016). Effects of vapour pressure on the motion of cavitation bubble. Phys. Chem. Liquids *55*, 1–10. https://doi.org/10.1080/00319104.2016.1163558.
67. Seeton, C.J. (2006). Viscosity-temperature correlation for liquids. In International joint tribology conference, pp. 133–144. https://doi.org/10.1115/IJTC2006-12139.
68. Fulem, M., Růžička, K., Růžička, V., Šimeček, T., Hulicius, E., and Pangrác, J. (2006). Vapour pressure measurement of metal organic precursors used for MOVPE. J. Chem. Thermodyn. *38*, 312–322. https://doi.org/10.1016/j.jct.2005.05.018.
69. Niemczewski, B. (2009). Influence of concentration of substances used in ultrasonic cleaning in alkaline solutions on cavitation intensity. Ultrason. Sonochem. *16*, 402–407. https://doi.org/10.1016/j.ultsonch.2008.09.002.

STAR★METHODS

KEY RESOURCES TABLE

REAGENT or RESOURCE	SOURCE	IDENTIFIER
Chemicals, peptides, and recombinant proteins		
50 cP liquid	Xilong Scientific Co.,Ltd.	N/A
100 cP liquid	Xilong Scientific Co.,Ltd.	N/A
150 cP liquid	Xilong Scientific Co.,Ltd.	N/A
200 cP liquid	Xilong Scientific Co.,Ltd.	N/A
Other		
NDJ-1 Rotational Viscometer	Shanghai Lichen Instrument Technology Co., Ltd.	N/A
AFG Signal generator	Tektronix, Inc.	N/A
HSA4051 Power amplifier	Negative Feedback, Inc.	N/A
DSO-X2004A Oscillograph	Keysight Technologies, Inc.	N/A
GPC3060D DC power supply	Guwei Electronics Co., Ltd	N/A
LabRAM HR Evolution	HORIBA Jobin Yvon, Inc.	N/A
VHX-5000 Ultradepth-of-field microscope	Keysight Technologies, Inc.	N/A
Winner311XP Laser particle size analyser	Jinan Winner Particle Instruments Stock Co., Ltd.	N/A
BHS-1 Water bath heater	JOANLAB Scientific Instrument Co., Ltd.	N/A
85-2 Magnetic stirrer	Shanghai Lichen Instrument Technology Co., Ltd.	N/A
FA2204 High-precision balance	Shanghai Lichen Instrument Technology Co., Ltd.	N/A

RESOURCE AVAILABILITY

Lead contact

The datasets generated or analyzed during the current study are available from the corresponding author on reasonable request, J. Zhang (zhangjh@nuaa.edu.cn).

Materials availability

This study did not generate new unique reagents.

Data and code availability

- Data reported in this paper will be shared by the lead contact upon reasonable request.
- This study does not report any original code.
- Any additional information required to reanalyze the data reported in this paper is available from the lead contact upon reasonable request.

METHOD DETAILS

Structure of the FTICA

The structure of this study is shown in the figure below, which consists of three parts: a drive source, a connecting block, and a liquid carrier. The vibration source includes a metal base and a piezoelectric ceramic, which is made by sintering $PbTiO_3$ series materials and is shown in baby blue in the figure below (A). The metal base, the connection block, and the liquid carrier are machined of 304 stainless steel. The

piezoelectric ceramic is bonded to the metal base with 3M DP460 epoxy resin, and the connection block is laser welded to the metal base and the liquid carrier. The main dimensions of the FTICA are shown in the table below.

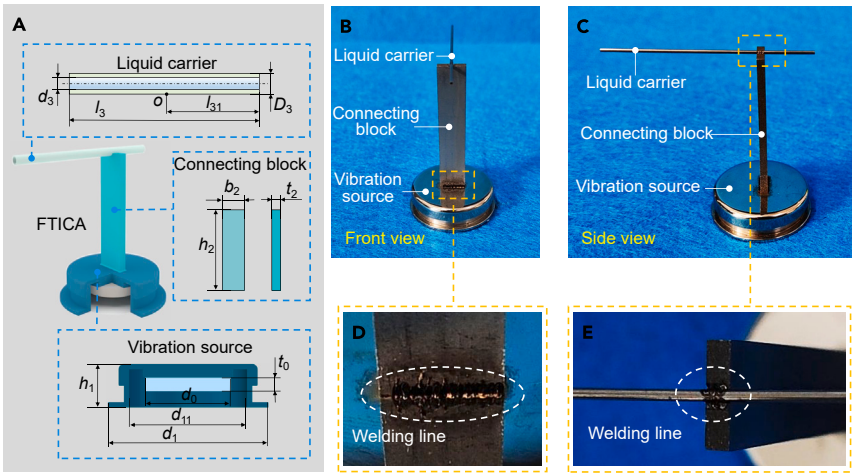

Structure of the FTICA

(A) schematic of the FTICA.

(B) photograph of the FTICA in front view.

(C) photograph of the FTICA in side view.

(D) welding area between the rectangular block and the metal base.

(E) welding area between the rectangular block and the liquid carrier.

Table Main dimensional values of the FTICA.

Parameters	Values
Diameter/d_0 (mm)	18.00
Thickness/t_0 (mm)	1.00
Diameter/d_1 (mm)	30.00
Diameter/d_{11} (mm)	24.00
Height/h_1 (mm)	8.00
Width/b_2 (mm)	9.00
Height/h_2 (mm)	36.00
Thickness/t_2 (mm)	2.00
Diameter/D_3 (mm)	1.00
Diameter/d_3 (mm)	0.80
Distance/l_3 (mm)	45.00
Distance/l_{31} (mm)	10.00

EXPERIMENTAL MODEL AND SUBJECT DETAILS

Impedance measurement experiment

Before conducting experiments on the effect of temperature and stirring rate on the atomization rate, experiments were conducted using an impedance analyzer (LCR Meter 6630, MICROTEST, Taiwan, China) for the same viscosity liquid at different temperatures and different stirring rates and measuring the impedance of the FTICA after passing different types of liquid. For example, the change in the temperature affects the liquidity of the liquid. However, determining whether flowability affects the stiffness of the FTICA, which results in a change in the resonant frequency of the FTICA, is the main purpose of the impedance analysis experiment. The experimental setup for impedance measurement is shown in the figure below.

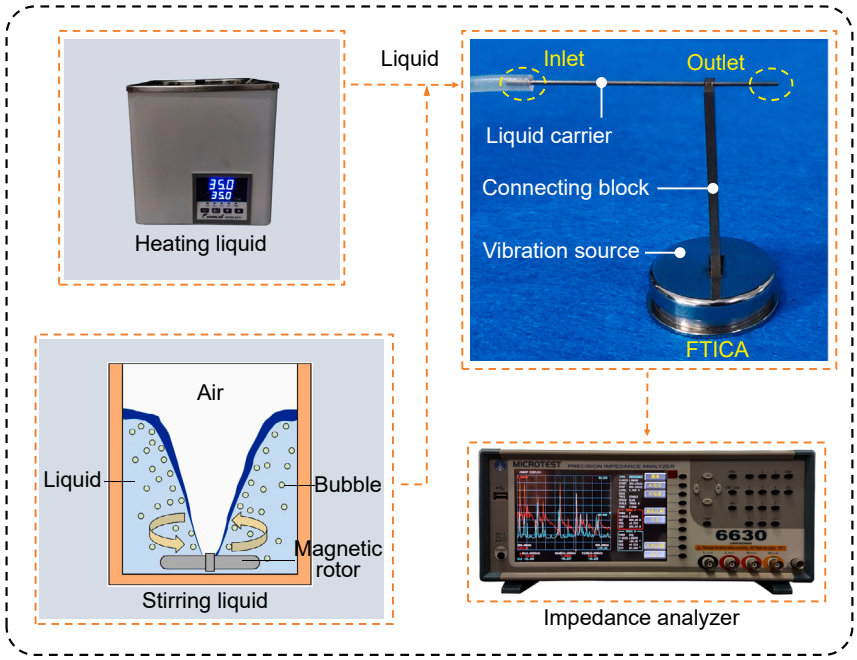

Experimental setup of impedance measurements

As shown in the figure above, the stirred and heated liquid was passed into the liquid carrier, and the FTICA impedance was measured using an impedance analyzer.

Experiments of viscosity analysis

In order to study the relationship between viscosity with temperature and gas content. First, the liquid is heated and stirred for 5 min, and them, a rotary viscometer (NDJ-1, LICHEN, Shanghai, China) was used to conduct experiments on the same viscosity liquid at different temperatures and different stirring rates, and to analyze the change of viscosity of the liquid in different environments. The experimental setup for viscosity measurement is shown in the figure below.

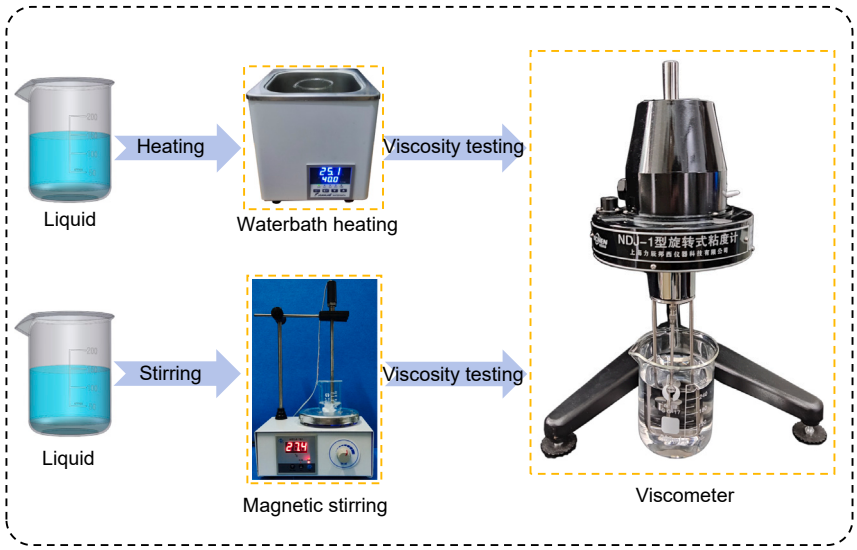

Experimental setup of viscosity measurement

Experiment of temperature and atomization rate

A water bath was used to heat the liquid to explore the relationship between temperature and atomization rate. Then, the atomization experiment was conducted. The experimental setup for heating atomization is shown in the figure below. In this study, a water bath heater (BHS-1,

JOANLAB, Zhejiang, China) was used to heat liquids with different viscosities and heat them for the same amount of time. Subsequently, a peristaltic pump was used to pump the liquid into the FTICA for atomization rate experiments. The drive signal of the FTICA was generated by a signal generator (AFG1022, Tektronix, Beaverton, WA, USA) and amplified and transmitted to the FTICA by a power amplifier (HAS4051, NF, Yokohama, Japan). An oscilloscope (DSOX2004A, Keysight, Santa Rosa, CA, USA) was used for simultaneous display to observe the changes in the input signal in real time. A high-precision balance (FA2204, LICHEN, Shanghai, China) was used to record the pumping volume at the maximum drive voltage of the peristaltic pump, which was the final atomization rate.

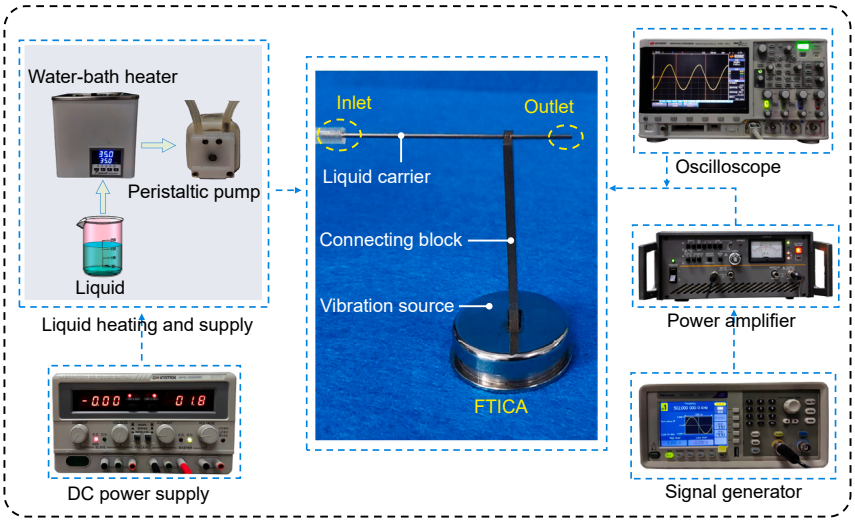

Experimental setup for liquid heating and atomization

The experimental setup for liquid heating and atomization is shown in the figure above, and this setup was used to perform atomization rate experiments at different temperatures. The atomization experiments were conducted at different temperatures with liquids of dynamic viscosities of 50, 100, 150, and 200 cP, and the atomization rates were measured at four temperatures of 25, 30, 35, and 40°C. For liquids of the same viscosity at the same temperature, the drive voltage of the AC signal was increased from 70 V to 80 V, and six sets of atomization rate measurements were completed at an interval of 2 V.

Experiment of temperature and stirring rate

The effect of the bubble number on the atomization rate was explored. First, a magnetic stirrer was used to stir liquids of different viscosities for the same time at room temperature. Then, the atomization experiment was performed on the stirred liquid, and the change in the

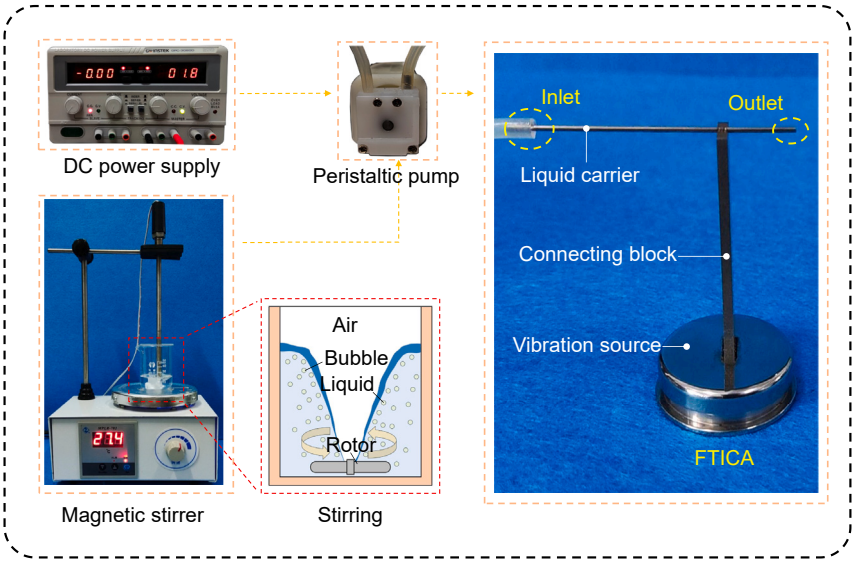

Experimental setup of stirring atomization

atomization rate was studied. The experimental setup of stirring atomization is shown in the figure below. This setup used a DC power supply (GPC-3060, GWINSTEK, Taiwan, China) to drive the peristaltic pump. Then, the stirred liquid was pumped to the FTICA to achieve atomization.

The experimental setup shown in the figure above was used to conduct the atomization experiments at different stirring rates. The stirring experiment was similar to the temperature experiment, which was divided into three groups of experiments according to the different stirring rates of 500, 1000, and 1500 r/min, respectively. The atomization experiments were conducted at different stirring rates for different viscosity liquids. Finally, the atomization rate was recorded.

This experiment was conducted to observe the stirred liquid with an ultradepth-of-field microscope (VHX-5000, KEYENCE, Osaka, Japan) and compare the changes in the number of bubbles at different stirring rates for better demonstrating the relationship between the stirring rate and the number of bubbles. The bubble observation setup of the ultradepth-of-field microscope is shown in the figure below.

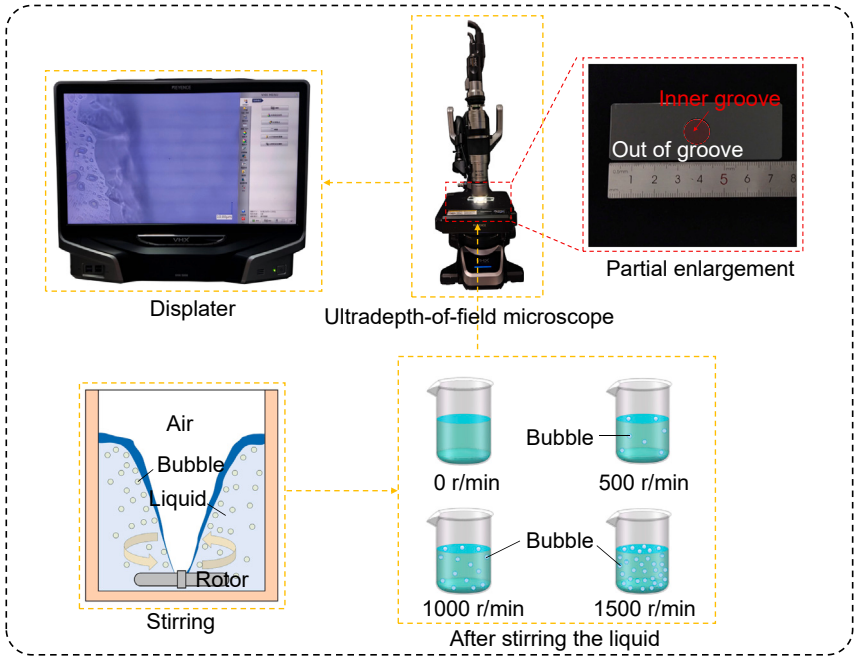

Diagram of the bubble observation setup of an ultradepth-of-field microscope

As shown in the figure above, the liquid with a dynamic viscosity of 50 cP was divided into four groups with the stirring rate as the independent variable: 0, 500, 1000, and 1500 r/min, respectively. The four groups of liquids were stirred for 5 min using a magnetic stirring device, and the stirred liquids were allowed to stand for 1 min before being placed on slides to observe the bubble density using an ultradepth-of-field microscope.

The diameter of the bubbles in the liquid is approximately 3 μm. Thus, an ultradepth-of-field microscope magnification was set to 2500×, after which fine adjustments were made to observe the bubble density inside the liquid. The liquid is difficult to focus directly at high flow speeds. Therefore, the lens was focused on the boundary between the liquid and the slide, and the bubble density could be observed within the visual range.

Experiment of Raman spectral analysis

In order to verify the chemical properties of the liquids after heating and stirring, and the safety of the FTICA atomization products after the heating and stirring treatment, a Laser Raman Spectrometer (LabRAM HR Evolution, HORIBA FRANCE SAS, France) was selected as the experimental setup for this study, and the wavelength of the laser light source was 532 nm. Firstly, Raman spectroscopy was performed to observe the chemical properties of the liquids after the heating and stirring treatment. Later, the products of FTICA atomization of the heated and stirred liquids are subjected to Raman spectroscopy. The experimental setup for Raman spectral analysis is shown in the figure below.

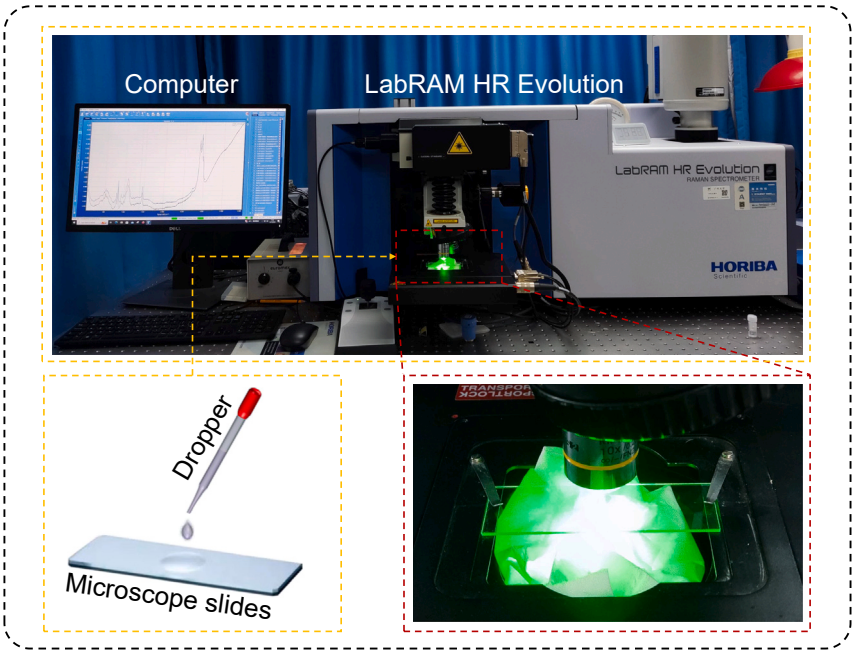

Experimental setup for Raman spectral analysis

Experiments on the relationship between temperature and atomized particles

In order to explore the relationship between temperature and atomized particles of FTICA, a laser particle size analyzer (Winner311XP, Winner Particle, Jinan, China) was used to test the atomized particles, and the experimental setup is shown in the figure below. Experiments were conducted at temperatures of 25°C, 30°C, 35°C and 40°C with a dynamic viscosity of 100 cP, and the diameter of atomized particles of FTICA was measured at four sets of different temperatures. The FTICA drive voltage is set to 76 V and the drive frequency to 507 kHz, the liquid is heated in a water bath and transported to the FTICA for atomization. A signal generator is used to output the AC signal, a power amplifier is used to amplify the AC signal, an oscilloscope is used to monitor the signal in real time, and the atomization outlet of the FTICA is aligned with the inlet of the laser particle sizer.

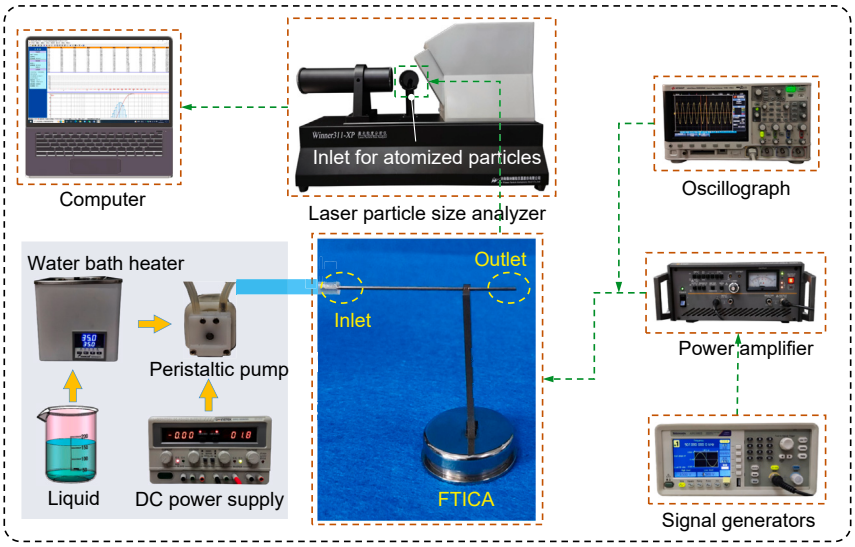

Experimental setup for heating atomized particles measurement

Experiments on the relationship between stirring and atomized particles

In order to explore the relationship between stirring and atomized particles of FTICA, a laser particle size analyzer (Winner311XP, Winner Particle, Jinan, China) was used to test the atomized particles, and the experimental setup is shown in the figure below. Experiments were conducted at stirring of 0 r/min, 500 r/min, 1000 r/min and 1500 r/min with a dynamic viscosity of 100 cP, and the diameter of atomized particles of FTICA was measured at four sets of different temperatures. The FTICA drive voltage is set to 76 V and the drive frequency to 507 kHz, the liquid is stirred in a magnetic stirrer and transported to the FTICA for atomization. A signal generator is used to output the AC signal, a power amplifier is used to amplify the AC signal, an oscilloscope is used to monitor the signal in real time, and the atomization outlet of the FTICA is aligned with the inlet of the laser particle sizer.

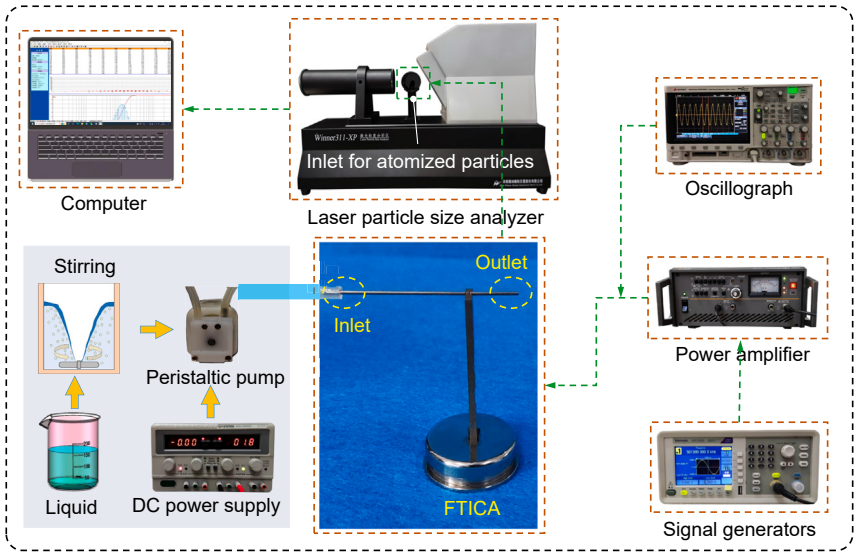

Experimental setup for stirring atomized particles measurement